Heinonen, J.S., Spera, F.J., and Bohrson, W.A., 2021, Thermodynamic limits for assimilation of silicate crust in primitive magmas: Geology, https://doi.org/10.1130/G49139.1

Thermodynamic limits for assimilation of silicate crust in primitive magmas

Jussi S. Heinonen[1], Frank J. Spera[2], and Wendy A. Bohrson[3]

[1]*Department of Geosciences and Geography, University of Helsinki, P.O. Box 64, 00014 Helsinki, Finland (jussi.s.heinonen@helsinki.fi)*

[2]*Department of Earth Science and Institute for Crustal Studies, University of California, Santa Barbara, CA, 93106, USA*

[3]*Department of Geology and Geological Engineering, Colorado School of Mines, Golden, CO, 80401 USA*

Supplemental Materials

INPUT PARAMETERS FOR MAGMA CHAMBER SIMULATOR MODELING

Details for modeling phase equilibria and major elements in open igneous systems using the Magma Chamber Simulator (MCS) are given in Bohrson et al. (2014, 2020); only features and parameters relevant to the current study are described here. Additional information regarding the MCS may be found in the cited references and at https://mcs.geol.ucsb.edu.

The input parameters for the simulations have been selected so that the *maximum* amount of assimilation allowed by thermodynamic constraints could be studied. In MCS, it is possible to model magmatic assimilation using two different methods: 1) assimilation of wall-rock anatectic (partial) melts and fractional crystallization (MCS-AFC) and 2) bulk or wholesale assimilation of stoped wall-rock blocks and fractional crystallization (MCS-SFC).

For MCS-AFC, sensible (melt cooling) and latent heat (released by crystallization) generated in the M subsystem is transferred through the magma body-wallrock diabatic boundary and heats up and potentially partially melts wallrock. Progressive batches of anatectic melt formed above a user-input percolation threshold for the wallrock are thoroughly mixed and equilibrated with the resident melt in discrete steps until magma and the wallrock reach thermal equilibrium and the simulation comes to a halt.

For MCS-SFC, a user-input mass of stoped wallrock is thoroughly mixed and equilibrated with the resident melt during one step, and the contaminated system comes to a new equilibrium state at a new temperature governed by thermodynamics. The stoping event may cause crystallization and/or separation of a fluid phase and the resulting compositional changes are recorded by the resident melt composition. The introduction of a stoped block is modeled using the recharge function of MCS; the MCS version used for the MCS-SFC cases here can handle up to thirty separate stoping events in a single simulation.

The simulations reported in this study are isobaric and modeled at pressures relevant to the different crustal environments: 800 MPa for simulations with lower crustal (LC) wall-rock, 500 MPa for simulations with middle crustal (MC) wall-rock, and 200 MPa for simulations with upper crustal (UC) wall-rock. These pressures correspond to depths of ~30, ~20 and ~7 km, respectively. Temperature decrement step for fractional crystallization mode in all the simulations is 5 °C (Bohrson et al., 2020). From preliminary testing, smaller decrements do not make a notable difference in the results. At the end of each step, the solids (± fluids) formed in equilibrium with the resident melt are fractionated from the resident magma. Wallrock partial melt is always in equilibrium with the residual wallrock solids (± fluids).

Parental melt parameters

The parental melts were selected to sample a wide variety of ages and geological environments (Table S1). The goal is to study the role compositionally distinct parental melts play in the efficiency of assimilation from the thermodynamic vantage, not to describe an actual assimilation scenario for a specific magmatic system. This is also why trace element or isotopic models are not presented.

The initial Fe^{2+}/Fe^{tot} (fO_2) was specified according to the constraints given in the sources and, if not given, secondarily using a ferrous/ferric ratio relevant to the given setting. Reasonable variations in initial Fe^{2+}/Fe^{tot} in the parental melt do not generally affect the model outcomes markedly in terms of liquidus T and thus enthalpy in mafic-ultramafic systems (see Heinonen et al., 2019). Note that an oxygen buffer was not imposed during the simulations, i.e., the magma-wallrock system remained closed with respect to oxygen loss or addition.

The initial H_2O contents of the parental melts were prescribed based on the original sources, if such information was given. However, the majority of the komatiitic, picritic, and basaltic LIP, OIB, and MORB parental melts were considered dry, because no information on the water contents was readily available. Water contents in these types of melts are nevertheless expected to be low (< 0.5 wt%). For the arc-related high-Mg basaltic parental melts, we used a H_2O content of 2 wt%, which is the lower limit of the global range shown by mafic arc magmas (H_2O = 2−6 wt%; Plank et al., 2013). Using a low estimate for the H_2O content is relevant when testing for thermodynamic limits of assimilation – using higher initial H_2O contents for the parental melt would mean less assimilation before thermal equilibration with the wallrock in the MCS-AFC simulations due to lowered liquidus T of the parental melt (Fig. S1). This effect is especially pronounced in models with lower crustal wallrock that has a high solidus T (Fig. S1). Adding reasonably small amounts of CO_2 in the parental melts would not be expected to change the results in any significant way.

Table S1. Parental melt compositions used in the MCS simulations

Komatiitic/meimechiitic

PM	*Location*	*Era*	*Source*	*Notes*
K01	Paraná-Etendeka LIP	Mesozoic	Thompson and Gibson (2000)	Parental magma for Hooringbai picritic dikes (Hooringbai parental komatiite); Fe^{2+}/Fe^{tot} = 0.9
K02	Karoo LIP	Mesozoic	Heinonen and Luttinen (2010)	Karoo meimechite parental magma "m1"; 1 wt% H_2O; Fe^{2+}/Fe^{tot} = 0.9
K03	Siberian Traps LIP	Paleozoic	Elkins-Tanton et al. (2007)	SYNS2 synthetic starting composition; 1 wt% H_2O; Fe^{2+}/Fe^{tot} = 0.9
K04	Gorgona Island	Mesozoic	Révillon et al. (2000)	GOR 512 "picrite", MgO closest to that projected for the parental magma; Fe^{2+}/Fe^{tot} = 0.9
K05	Emeishan LIP	Paleozoic	Hanski et al. (2004)	Sample B6865 from Song Da (Vietnam), MgO closest to that projected for the parental magma (22.5 wt%); Fe^{2+}/Fe^{tot} = 0.9
K06	Belingwe Greenstone Belt	Neoarchean	Renner (1989)	bulk flow composition, listed as a komatiite liquid in Nisbet et al. (1993); Fe^{2+}/Fe^{tot} = 0.9
K07	Abitibi Greenstone Belt	Neoarchean	Arndt (1986)	Sample M666, listed as a komatiite liquid in Arndt et al. (2008); Fe^{2+}/Fe^{tot} = 0.9
K08	Barberton Greenstone Belt	Paleo-archean	Parman et al. (2004)	Sample K4-1BA, listed as a komatiite liquid in Arndt et al. (2008); Fe^{2+}/Fe^{tot} = 0.9
K09	Commondale Greenstone Belt	Paleo-archean	Wilson (2003)	listed as a komatiite liquid in Arndt et al. (2008); Fe^{2+}/Fe^{tot} = 0.9
K10	Norseman–Wiluna Greenstone Belt	Neoarchean	Lewis and Williams (1973)	listed as a komatiite liquid in Arndt et al. (2008); Fe^{2+}/Fe^{tot} = 0.9

Picritic

PM	*Location*	*Era*	*Source*	*Notes*
P01	Gorgona Island	Mesozoic	Herzberg and O'Hara (2002)	Model Gorgona "komatiite" parental magma formed by accumulated perfect fractional melting; Fe^{2+}/Fe^{tot} as measured
P02	Grassy Portage Bay Greenstone Belt	Neoarchean	Goldstein and Francis (2008)	GP-10 pyroclastic ferropicrite; Fe^{2+}/Fe^{tot} = 0.9
P03	North Atlantic Igneous Province	Cenozoic	Larsen and Pedersen (2009)	Parental melt calculated for the Aaanaa Mb, Vaigat Fm, West Greenland; Fe^{2+}/Fe^{tot} = 0.9
P04	Hawaii	Cenozoic	Norman and Garcia (1999)	Sample KIL-1-7 that corresponds to Kilauea parental magma composition with MgO of ~16 wt% and Al_2O_3 of ~10 wt%; Fe^{2+}/Fe^{tot} = 0.9
P05	Karoo LIP	Mesozoic	Sweeney et al. (1991)	Fertile Mwenezi picrite low-K (low-NaK# HTZ group) end-member; 1 wt% H_2O (see Liu et al., 2017); Fe^{2+}/Fe^{tot} as measured

P06	Ontong Java Plateau	Mesozoic	Herzberg et al. (2007)	Primary magma for sample 1187-8 from Fitton and Godard (2004); Fe^{2+}/Fe^{tot} as measured
P07	Ferrar LIP	Mesozoic	Sweeney et al. (1991)	Parental Ferrar composition (Ortez and Green, unpubl. data, LTZ group); Fe^{2+}/Fe^{tot} as measured
P08	Deccan LIP	Mesozoic	Krishnamurthy (1974)	A representative high-Mg picrite sample (see Krishnamurthy et al., 2000); Fe^{2+}/Fe^{tot} = 0.9
P09	Siberian Traps LIP	Paleozoic	Lightfoot et al. (1993)	Tuklonsky Fm picrite 1F(30); Fe^{2+}/Fe^{tot} = 0.9
P10	Siberian Traps LIP	Paleozoic	Lightfoot et al. (1993)	Gudchichinsky Fm picrite 1F(18); Fe^{2+}/Fe^{tot} = 0.9

Basaltic

PM	*Location*	*Era*	*Source*	*Notes*
B01	Vanuatu arc	Cenozoic	Eggins (1993)	The most primitive aphyric lava sample #68638 from Manaro Voui (Ambae); 2 wt% H_2O (Plank et al., 2013); Fe^{2+}/Fe^{tot} = 0.7 (~QFM +2)
B02	Early Central American Volcanic Arc System	Cenozoic	Whattam (2018)	Primitive sample PAN-03-016; 2 wt% H_2O (Plank et al., 2013); Fe^{2+}/Fe^{tot} = 0.8
B03	Kurile-Kamchatka volcanic arc	Cenozoic	Portnyagin et al. (2005)	Parental melt of avachites (AV-I) based on melt inclusions in olivine; 2 wt% H_2O (Plank et al., 2013); Fe^{2+}/Fe^{tot} = 0.8
B04	Iceland	Cenozoic	Breddam (2002)	Most primitive olivine tholeiitic glasses found in central Iceland (Kistufell); Fe^{2+}/Fe^{tot} = 0.9
B05	Southwest Indian Ridge	Cenozoic	Font et al. (2007)	Most primitive calculated parental melt composition (PM-DR51); 0.09 wt% H_2O; Fe^{2+}/Fe^{tot} = 0.9
B06	Hawaii	Cenozoic	Frey et al. (1991)	Sample MU-8 from Maulua Gulch may be the most magnesian postshield tholeiitic lava that represents a crystallized melt; Fe^{2+}/Fe^{tot} = 0.9
B07	Pyrolite melt composition (experimental)	-	Jaques and Green (1980)	Calculated equilibrium melt composition at 1350 °C, 1.5 GPa, 18% melting; Fe^{2+}/Fe^{tot} as measured
B08	Aleutian arc	Cenozoic	Miller et al. (1992)	A composition similar to LUM21 is suggested as a parental magma for the Recheshnoi suite (Umnak); 2 wt% H_2O (Plank et al., 2013); Fe^{2+}/Fe^{tot} = 0.8
B09	Karoo LIP	Mesozoic	Heinonen and Luttinen (2008)	A low-degree picrobasaltic melt (sample 117-KHG-91) from a depleted source (see also Heinonen et al., 2010); Fe^{2+}/Fe^{tot} = 0.9
B10	Ethiopian-Yemeni LIP	Cenozoic	Beccaluva et al. (2009)	A depleted primitive basalt (LAL1) with low LOI (see also Natali et al., 2016 - Fe^{2+}/Fe^{tot} = 0.8 reported there)

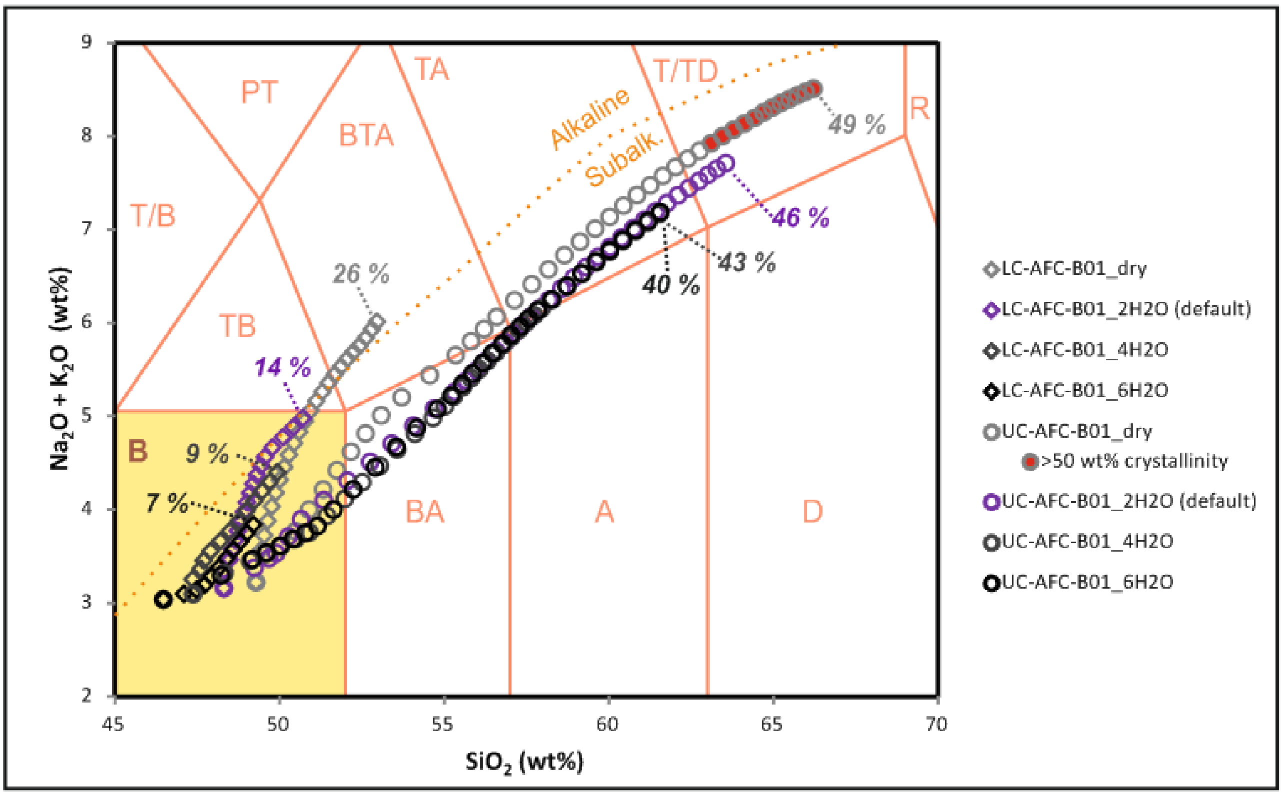

Figure S1. The results of the MCS-AFC simulations in which B01 parental melt with varying water content (0, 2, 4, and 6 wt%; 2 wt% are the default simulations shown in Figs. 1 and 2 and Table S2) assimilates LC or UC shown in SiO_2 vs. $Na_2O + K_2O$ (TAS) diagram (Le Bas et al., 1986). Each open symbol after the first one in the basalt field represents an assimilation step where wallrock partial melt above the percolation threshold of 10 wt% is homogenized with the resident melt. Results with >50 wt% crystallinity are highlighted and the stippled lines and numbers in italics indicate the total amount of assimilation (in wt% relative to the initial parental melt) in the end of the simulations. Abbreviations of the TAS classification: T/B = tephrite/basanite, B = basalt (highlighted in yellow), TB = trachybasalt, PT = phonotephrite, BA = basaltic andesite, BTA = basaltic trachyandesite, A = andesite, TA = trachyandesite, D = dacite, T/TD = trachyte/trachydacite, R = rhyolite.

Wallrock parameters

The wallrock compositions represent average modern LC, MC, and UC of Rudnick and Gao (2003). Initial H_2O contents are estimated at 0.9 wt% for UC (Johnson, 2006; Ni et al., 2017), 0.045 wt% for LC Yang et al. (2008; average of all samples), and 0.2 wt% for MC assuming exponential interpolation midway between UC and LC. Fe^{2+}/Fe^{tot} has been constrained at QFM at the liquidus temperature at a given pressure (800 MPa for LC, 500 MPa for MC, and 200 MPa for UC). In the

AFC simulations, the initial temperature of the wallrock was set above solidus but below percolation threshold ("FmZero") of 10 wt% melt (LC: melt fraction = 9.4 wt% at 1060 °C and 0.8 GPa; MC: melt fraction = 9.6 wt% at 880 °C and 0.5 GPa; UC: melt fraction = 6.9 wt% at 700 °C and 0.2 GPa), which represents a reasonable value for common crustal rocks (see Bohrson et al., 2014). After reaching the percolation threshold fraction of 0.1, the wall-rock remains 10 wt% molten throughout the simulation (and the wall-rock melt and residual solids remain in equilibrium). If, after a computational step the local melt fraction in WR exceeds 10 wt%, then the mass of anatectic melt removed is such that the post–removal melt fraction in WR returns to the 10 wt% threshold. In the MCS-SFC simulations, blocks of wallrock having the same initial supersolidus temperature as in in the respective MCS-AFC simulations are homogenized with the resident magma in 30 stoping events, each with a stoped mass of 5 units and with one fractional crystallization step in between.

In MCS-AFC, the heat released by the crystallizing magma is homogeneously distributed to the user-specified mass of wallrock; this is a thermodynamic model and thermal gradients are not explicitly modeled. Defining wallrock-magma ratio for MCS in various geologic contexts is discussed by Bohrson et al. (2014). Here, we preliminarily tested magma-wallrock mass ratios of 1:1, 1:2, and 1:3 for the case of parental melt K10 assimilating LC. These parental melt and wallrock compositions where chosen because of the high heat content of the melt and because the resident melt remains basaltic even at high degrees of assimilation. The results of the modeling are presented in resident magma temperature vs. amount of assimilation plot in Fig. S2.

For the magma-wallrock mass ratio of 1:1, the wallrock is efficiently assimilated and less than 30 wt% of solid residual wallrock remains when the Rhyolite-MELTS engine for the wallrock halts and cannot find a feasible solution. At this point, the T difference between the resident magma and the wallrock, now composed of 77 wt% clinopyroxene and 23 wt% plagioclase, is still more than 100 °C. We consider the ratio of 1:1 to be too small in pursuit of maximum amount of assimilation.

In addition, melting the wallrock to very high degree can destabilize the calculation. It should also be noted that because of the relatively low mass of the wallrock, assimilation in excess of 100 wt% would not be possible in this case, even if the simulation would proceed until magma-wallrock equilibration.

For the magma-wallrock mass ratio of 1:3, the melting of the wallrock requires a lot of heat from the crystallizing magma and thus assimilation is not very pronounced. When the simulation reaches equilibrium at ~1240 °C, less than 30 wt% of the initial wallrock mass (300 units) has been assimilated.

For the magma-wallrock mass ratio of 1:2, the simulation does not halt prematurely and the wallrock does not become excessively depleted early on (cf. the 1:1 case) and the assimilation proceeds relatively efficiently (cf. the 1:3 case) and exceeds 100 wt% at the end of the simulation. When the simulation reaches equilibrium at ~1280 °C, ~50 wt% of the initial wallrock mass (200 units) has been assimilated. We consider the magma-wallrock ratio of 1:2 to represent a reasonable compromise and use it in the simulations described in the text. This condition approximates the maximum limit for the magma-wallrock ratio in low-permeability rocks with very limited hydrothermal flow (Bohrson et al., 2014). Such conditions cause steep thermal gradients and induce notable partial melting in the wallrock, which is ideal for the purpose of this study.

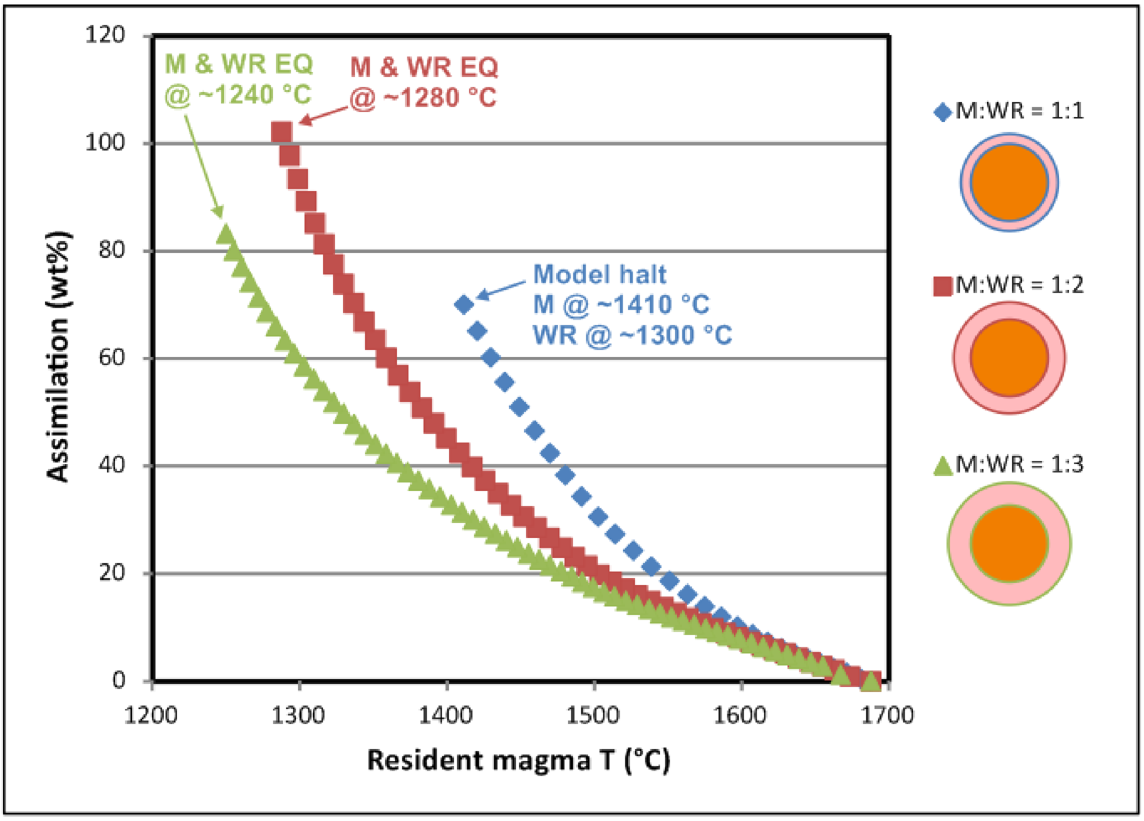

Figure S2. Resident magma temperature vs. amount of assimilation (relative to the initial mass of the parental melt) shown for three MCS-AFC cases of K10 parental melt assimilating LC wallrock. The cases differ in relative initial masses of the parental melt (always 100 mass units) and the wallrock (100, 200, or 300 mass units). The relative masses are also illustrated as crosscut spheres in the legend: the inner sphere represents the mass of the initial melt and the outer spherical shell represents the mass of the wallrock included in the simulation. Each symbol after the first one, which marks the initial setting at ~1700 °C, represents an assimilation step. M = resident magma, WR = wallrock, EQ = equilibrium.

ASSIMILATION OF PARTIAL MELTS (MCS-AFC MODELING) VERSUS BULK ASSIMILATION (MCS-SFC MODELING)

The MCS is a thermodynamic model and as such does not take account of dynamic, kinetic, or non-equilibrium effects. Although this may first appear to be a debilitating limitation, the collective results of over seventy years of petrological research clearly indicates that the thermodynamic approach is often an excellent approximation to geologic reality (Carmichael et al, 1974). Indeed, the phase equilibria approach, pioneered by N.L. Bowen over a century ago, is at the core of modern igneous petrology. Regarding assimilation, thermodynamic models provide an upper limit on the assimilant mass in scenarios where recharge plays no role. The existence of an upper limit is based on the foundational energetic constraint that wallrock heating and melting depends on the energy flow from magma to wallrock host. In MCS-SFC, stoped crystalline blocks of lower specific enthalpy (crystalline phase state and lower ambient temperature compared to magma) act as efficient heat sinks upon incorporation, whereas in MCS-AFC assimilant of high specific enthalpy (a partial melt rather than crystalline block) is less of a heat sink. The “heat sink” effect of MCS-SFC vs. MCS-AFC can be traced in MCS by noting in any given simulation the degree of crystallinity of the contaminated resident magma. That is, comparison of MCS-SFC and MCS-AFC models show that the mass of cumulates associated with the M sub system for MCS-SFC surpasses that of the MCS-AFC models at high degrees of assimilation (Fig. S3). MCS-AFC modeling should thus be a more viable method to trace *maximum* amounts of assimilation allowed by the primitive magmas, the primary goal of this study.

Unless the physical separation of melt and the formed crystals is efficient, the viscosity of magmas is expected to increase significantly at crystallinities of ~40−60 wt% (e.g., Shaw et al., 1968; Lejeune and Richet, 1995; Vigneresse et al., 1996; see also Glazner, 2007; Mueller et al, 2010; Truby et al, 2015). Although this is highly dependent on the timescales, dimensions, and dynamic and kinetic factors in the modeled open magma system, we consider crystallinity of 50 wt% as the threshold value in the simulations (Fig. S3). That is, in all the results of the MCS-AFC simulations presented in Figs. 1−3 and Table S2, the crystallinity of the assimilating magma is below 50 wt%.

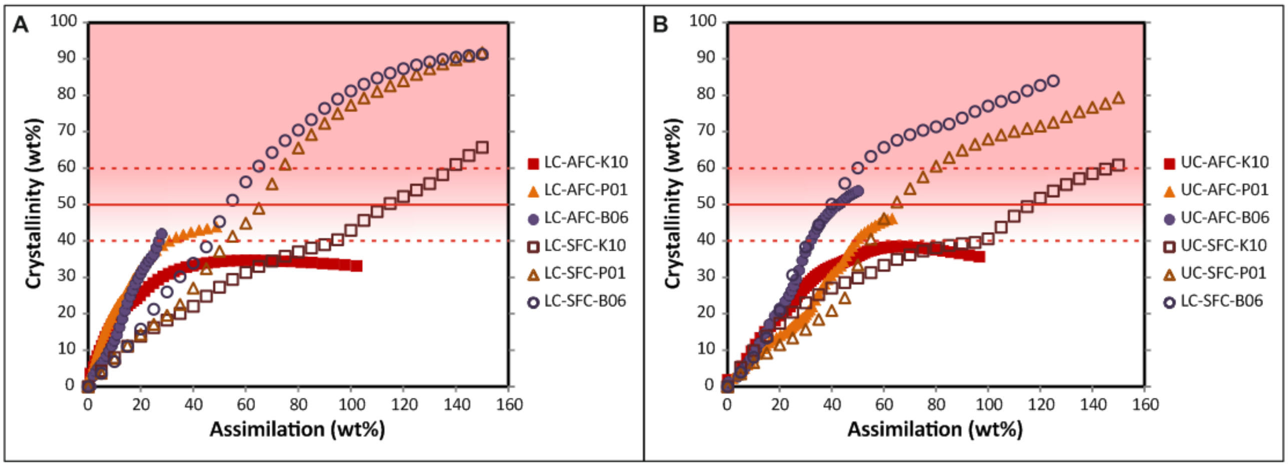

Figure S3. Amount of assimilation (relative to the initial mass of the parental melt) versus crystallinity of the resident magma chamber shown for MCS-AFC and MCS-SFC simulations of K10, P01, and B06 parental melts assimilating LC (A) and UC (B). Each symbol after the first one, which marks the initial setting at the origin, represents an assimilation step. Simulation UC-AFC-B06 is one of the few MCS-AFC simulations in which crystallinity surpasses 50 wt%. In this case, this takes place in resident melt composition more siliceous than basaltic. For MCS-AFC simulations LC-AFC-B04 and LC-AFC-B05 (not shown here) crystallinities surpass 50 wt% while the resident melt is basaltic and the respective results above that value are thus not included in the considerations presented in the main article (Figs. 1−3).

FULL LISTING OF THE MAGMA CHAMBER SIMULATOR SIMULATIONS

The full input and output of the MCS simulations is stored as Microsoft Excel worksheets in a zip file. The worksheets have been cleaned from most of the MCS-generated chart tabs (“ChartMassFrac”, “ChartPPD”, “ChartPMD”, “Charts”, and “XChartDiagramsData”) to fit the supplement size requirements of Geology. Table S2 lists selected numerical output that was used to construct the histogram in Fig. 2 in the main article. The list of all the output files is provided below in Table S3 and appended with relevant notes. For each output file, the simulation input is given in the “Input” tab and the major element and phase equilibria evolution of the simulations are recorded in the “RunSummary” tab. Note that not all the simulations were able to run until equilibrium (in the case of MCS-AFC) or user defined hard stop temperature (in the case of MCS-SFC; hard stop T given in the input), but halted because the Rhyolite-MELTS engine did not find a solution for a particular composition at the given conditions. If this happened late in the run, it makes no difference for the purpose of this study, but for some cases we had to slightly alter the wallrock initial mass parameters (± 5 units) in order for the simulations to avoid computational dead ends early in the simulations. These are clearly marked in the notes.

All MCS-AFC simulations have been run with MCS version PhaseEQ_2019AC and using Rhyolite-MELTS engine v.1.2.0. The MCS-SFC simulations use the same Rhyolite-MELTS engine, but a different version of MCS PhaseEQ_2019AH, which allows up to 30 recharge (stoping) events. The thermodynamic workings of the two MCS versions are identical. For more information, visit the MCS website at https://mcs.geol.ucsb.edu/.

Table S2. Parental melt compositions and results of the Magma Chamber Simulator modeling

Parental melt (PM)	PM Type	PM MgO (wt%)	MAX A (KOM/MEI) LC / MC / UC (wt%)[a]	MAX A (PIC) LC / MC / UC (wt%)[a]	MAX A (BAS) LC / MC / UC (wt%)[a]
Komatiitic/meimechitic parent undergoing AFC to komatiite/meimechite, picrite, and basalt					
Etendeka LIP	KOM	24	9 / 9 / 12	22 / 23 / 17	67 / 24 / -
Karoo LIP	MEI	25	9 / 12 / 13	24 / 24 / 24	59 / - / -
Siberian Traps	MEI	27	12 / 15 / 16	31 / 29 / 29	66 / 32 / 33
Gorgona	KOM	25	9 / 10 / 13	23 / 25 / 21	71 / 26 / -
Emeishan LIP	KOM	23	7 / 9 / 10	21 / 23 / 20	67 / 26 / -
Belingwe GB	KOM	26	11 / 12 / 13	26 / 16 / -	72 / - / -
Abitibi GB	KOM	28	16 / 17 / 19	33 / 25 / 19	85 / - / -
Barberton GB	KOM	30	20 / 21 / 15	39 / - / -	91 / - / -
Commondale GB	KOM	31	21 / 4 / 6	39 / - / -	92 / - / -
Norseman–Wiluna GB	KOM	34	27 / 24 / 24	51 / - / -	102 / - / -
AVERAGE		**27**	**14 / 13 / 14**	**31 / 24 / 22**	**77 / 27 / 33**
Picritic parent undergoing AFC to picrite and basalt					
Gorgona	PIC	19	-	11 / 13 / 15	49 / 28 / 20
Grassy Portage Bay GB	PIC (FP)	19	-	11 / 13 / 15	44 / 41 / 28
NAIP	PIC	18	-	10 / 11 / 13	45 / 28 / 16
Hawaii	PIC	16	-	6 / 8 / 9	40 / 21 / -
Karoo LIP	PIC	15	-	5 / 5 / 7	28 / 18 / 13
Ontong Java	PIC	17	-	7 / 9 / 11	42 / 21 / 13
Ferrar LIP	PIC	15	-	5 / 6 / 5	28 / 12 / -
Deccan LIP	PIC	17	-	6 / 8 / 10	38 / 26 / 21
Siberian Traps	PIC	17	-	7 / 9 / 11	41 / 27 / 13
Siberian Traps	PIC (FP)	18	-	8 / 11 / 12	45 / 34 / 17
AVERAGE		**17**		**8 / 9 / 11**	**40 / 26 / 18**
Basaltic/picrobasaltic parent undergoing AFC to basalt					
Vanuatu arc	BAS	10	-	-	14 / 13 / 11
Early Central Am. arc	BAS	12	-	-	15 / 17 / 17
Kurile-Kamchatka arc	BAS	10	-	-	11 / 12 / 15
Iceland	BAS	10	-	-	18[b] / 18 / 15
Southwest Indian Ridge	BAS	10	-	-	14[b] / 18 / 13
Hawaii	BAS	11	-	-	25 / 22 / 20
Pyrolite melt	BAS	12	-	-	11 / 12 / 11
Aleutian arc	BAS	10	-	-	14 / 10 / 9
Karoo LIP	PBAS	11	-	-	22 / 21 / 25
Ethiopian-Yemeni LIP	BAS	10	-	-	14 / 13 / 16
AVERAGE		**11**			**18 / 16 / 15**

Abbreviations in the order of appearance: LIP = Large igneous province, GB = Greenstone belt, KOM = komatiitic, MEI = meimechiitic, PIC = picritic, FP = ferropicritic, BAS = basaltic, PBAS = picrobasaltic, A = assimilation, LC = lower crust, MC = middle crust, UC = upper crust

[a] Maximum amount of partial melt assimilation of LC/MC/UC at a given melt composition (KOM/MEI: MgO > 18 wt%, SiO_2 < 52 wt%, alkalis not considered; PIC: MgO = 12−18 wt%, SiO_2 < 52 wt%, alkalis not considered; BAS: MgO < 12 wt%, SiO_2 < 52 wt%, $Na_2O + K_2O$ < 5 wt%; Le Bas et al., 1986; Le Bas, 2000) and below <50 wt% of crystallinity of the resident magma in the model. Averages exclude the results without a value marked with "-" (i.e., those that have evolved outside of the listed classification scheme).

[b] Assimilation above this value in the basaltic field happens at crystallinities >50 wt% and is thus not reported

Table S3. The list of the MCS-AFC and MCS-SFC simulations (naming: “assimilant”-“process”-“parental melt”).

Simulation	*Notes*
LC-AFC-B01	
LC-AFC-B01_4H2O	4 wt% of H_2O in the parental melt, only used in Fig. S1
LC-AFC-B01_6H2O	6 wt% of H_2O in the parental melt, only used in Fig. S1
LC-AFC-B01_dry	0 wt% of H_2O in the parental melt, only used in Fig. S1
LC-AFC-B02	
LC-AFC-B03	
LC-AFC-B04	crystallinity of 50 wt% surpassed in the basaltic field
LC-AFC-B05	crystallinity of 50 wt% surpassed in the basaltic field
LC-AFC-B06	
LC-AFC-B07	initial wallrock mass = 205 mass units
LC-AFC-B08	
LC-AFC-B09	initial wallrock mass = 195 mass units
LC-AFC-B10	
LC-AFC-K01	
LC-AFC-K02	
LC-AFC-K03	
LC-AFC-K04	initial wallrock mass = 205 mass units
LC-AFC-K05	
LC-AFC-K06	
LC-AFC-K07	
LC-AFC-K08	
LC-AFC-K09	
LC-AFC-K10	
LC-AFC-K10_m100	only used in Fig. S2; initial wallrock mass = 100 mass units; halted before magma-wallrock equilibration
LC-AFC-K10_m300	only used in Fig. S2; initial wallrock mass = 300 mass units
LC-AFC-P01	
LC-AFC-P02	
LC-AFC-P03	
LC-AFC-P04	
LC-AFC-P05	
LC-AFC-P06	
LC-AFC-P07	
LC-AFC-P08	
LC-AFC-P09	
LC-AFC-P10	
LC-SFC-B06	only used for Fig. S3
LC-SFC-K10	only used for Fig. S3
LC-SFC-P01	only used for Fig. S3

MC-AFC-B01
MC-AFC-B02
MC-AFC-B03
MC-AFC-B04
MC-AFC-B05
MC-AFC-B06
MC-AFC-B07
MC-AFC-B08
MC-AFC-B09
MC-AFC-B10

MC-AFC-K01
MC-AFC-K02
MC-AFC-K03
MC-AFC-K04
MC-AFC-K05
MC-AFC-K06
MC-AFC-K07
MC-AFC-K08
MC-AFC-K09
MC-AFC-K10

MC-AFC-P01
MC-AFC-P02
MC-AFC-P03
MC-AFC-P04
MC-AFC-P05
MC-AFC-P06
MC-AFC-P07
MC-AFC-P08
MC-AFC-P09
MC-AFC-P10

UC-AFC-B01	
UC-AFC-B01_4H2O	4 wt% of H_2O in the parental melt, only used in Fig. S1
UC-AFC-B01_6H2O	6 wt% of H_2O in the parental melt, only used in Fig. S1
UC-AFC-B01_dry	0 wt% of H_2O in the parental melt, only used in Fig. S1
UC-AFC-B02	
UC-AFC-B03	
UC-AFC-B04	
UC-AFC-B05	
UC-AFC-B06	
UC-AFC-B07	
UC-AFC-B08	
UC-AFC-B09	
UC-AFC-B10	

UC-AFC-K01	halted before magma-wallrock equilibration
UC-AFC-K02	
UC-AFC-K03	
UC-AFC-K04	
UC-AFC-K05	
UC-AFC-K06	
UC-AFC-K07	
UC-AFC-K08	
UC-AFC-K09	
UC-AFC-K10	
UC-AFC-P01	
UC-AFC-P02	
UC-AFC-P03	
UC-AFC-P04	
UC-AFC-P05	
UC-AFC-P06	
UC-AFC-P07	
UC-AFC-P08	
UC-AFC-P09	
UC-AFC-P10	
UC-SFC-B06	only used in Fig. S3; halted after 25 S events
UC-SFC-K10	only used in Fig. S3
UC-SFC-P01	only used in Fig. S3; halted before hard stop temperature

REFERENCES CITED

Arndt, N.T., 1986, Differentiation of Komatiite Flows. Journal of Petrology, v. 27, no. 2, p. 279–301. doi:10.1093/petrology/27.2.279.

Arndt, N., Lesher, C.M., and Barnes, S.J., 2008, Komatiite. Cambridge, Cambridge University Press.

Beccaluva, L., Bianchini, G., Natali, C., and Siena, F., 2009, Continental Flood Basalts and Mantle Plumes: a Case Study of the Northern Ethiopian Plateau. Journal of Petrology, v. 50, no. 7, p. 1377–1403. doi:10.1093/petrology/egp024.

Bohrson, W.A., Spera, F.J., Ghiorso, M.S., Brown, G.A., Creamer, J.B., and Mayfield, A., 2014, Thermodynamic Model for Energy-Constrained Open-System Evolution of Crustal Magma Bodies Undergoing Simultaneous Recharge, Assimilation and Crystallization: the Magma Chamber Simulator. Journal of Petrology, v. 55, no. 9, p. 1685–1717. doi:10.1093/petrology/egu036.

Bohrson, W.A., Spera, F.J., Heinonen, J.S., et al., 2020, Diagnosing open-system magmatic processes using the Magma Chamber Simulator (MCS): part I—major elements and phase equilibria. Contributions to Mineralogy and Petrology, v. 175, no. 11, 104. doi:10.1007/s00410-020-01722-z.

Breddam, K., 2002, Kistufell: Primitive Melt from the Iceland Mantle Plume. Journal of Petrology, v. 43, no. 2, p. 345−373. doi:10.1093/petrology/43.2.345.

Carmichael, I.S., Turner, F.J., and Verhoogen, J., 1974, Igneous petrology. New York, USA, McGraw-Hill, 739 p

Eggins, S.M., 1993, Origin and differentiation of picritic arc magmas, Ambae (Aoba), Vanuatu. Contributions to Mineralogy and Petrology, v. 114, no. 1, p. 79−100. doi:10.1007/BF00307867.

Elkins-Tanton, L.T., Draper, D.S., Agee, C.B., Jewell, J., Thorpe, A., and Hess, P.C., 2007, The last lavas erupted during the main phase of the Siberian flood volcanic province: results from experimental petrology. Contributions to Mineralogy and Petrology, v. 153, no. 2, p. 191−209. doi:10.1007/s00410-006-0140-1.

Fitton, J.G., and Godard, M., 2004, Origin and evolution of magmas on the Ontong Java Plateau. *in* Fitton, J.G., Mahoney, J.J., Wallace, P.J. and Saunders, A.D., eds., Origin and Evolution of the Ontong Java Plateau, Geological Society, London, Special Publication, v. 229, p.151−178. doi:10.1144/GSL.SP.2004.229.01.10.

Font, L., Murton, B.J., Roberts, S., and Tindle, A.G., 2007, Variations in Melt Productivity and Melting Conditions along SWIR (70°E–49°E): Evidence from Olivine-hosted and Plagioclase-hosted Melt Inclusions. Journal of Petrology, v. 48, no. 8, p. 1471−1494. doi:10.1093/petrology/egm026.

Frey, F.A., Garcia, M.O., Wise, W.S., Kennedy, A., Gurriet, P., and Albarede, F., 1991, The evolution of Mauna Kea Volcano, Hawaii; petrogenesis of tholeiitic and alkalic basalts. Journal of Geophysical Research, v. 96, no. B9, p. 14,347−14,375.

Glazner, A.F., 2007, Thermal limitations on incorporation of wall rock into magma. Geology, v. 35, no. 4, p. 319−322. doi:10.1130/G23134A.1.

Goldstein, S.B., and Francis, D., 2008, The petrogenesis and mantle source of Archaean ferropicrites from the Western Superior Province, Ontario, Canada. Journal of Petrology, v. 49, no. 10, p. 1729−1753. doi:10.1093/petrology/egn044.

Hanski, E., Walker, R.J., Huhma, H., Polyakov, G.V., Balykin, P.A., Tran, T.H., and Ngo, T.P., 2004, Origin of the Permian-Triassic komatiites, northwestern Vietnam. Contributions to Mineralogy and Petrology, v. 147, no. 4, p. 453−469. doi:10.1007/s00410-004-0567-1.

Heinonen, J.S., and Luttinen, A.V., 2010, Mineral chemical evidence for extremely magnesian subalkaline melts from the Antarctic extension of the Karoo large igneous province. Mineralogy and Petrology, v. 99, no. 3, p. 201−217. doi:10.1007/s00710-010-0115-9.

Heinonen, J.S., Carlson, R.W., and Luttinen, A.V., 2010, Isotopic (Sr, Nd, Pb, and Os) composition of highly magnesian dikes of Vestfjella, western Dronning Maud Land, Antarctica: A key to the origins of the Jurassic Karoo large igneous province?. Chemical Geology, v. 277, no. 3-4, p. 227-244. doi:10.1016/j.chemgeo.2010.08.004.

Heinonen, J.S., and Luttinen, A.V., 2008, Jurassic dikes of Vestfjella, western Dronning Maud Land, Antarctica: Geochemical tracing of ferropicrite sources. Lithos, v. 105, no. 3−4, p. 347−364. doi:10.1016/j.lithos.2008.05.010.

Heinonen, J.S., Luttinen, A.V., Spera, F.J., and Bohrson, W.A., 2019, Deep open storage and shallow closed transport system for a continental flood basalt sequence revealed with Magma Chamber Simulator. Contributions to Mineralogy and Petrology, v. 174, no. 11, 87. doi:10.1007/s00410-019-1624-0.

Herzberg, C., Asimow, P.D., Arndt, N.T., et al., 2007, Temperatures in ambient mantle and plumes; constraints from basalts, picrites, and komatiites. Geochemistry, Geophysics, Geosystems, v. 8, no. 2 doi:10.1029/2006GC001390.

Herzberg, C., and O'Hara, M.J., 2002, Plume-associated ultramafic magmas of Phanerozoic age. Journal of Petrology, v. 43, no. 10, p. 1857−1883. doi:10.1093/petrology/43.10.1857.

Jaques, A.L., and Green, D.H., 1980, Anhydrous melting of peridotite at 0–15 Kb pressure and the genesis of tholeiitic basalts. Contributions to Mineralogy and Petrology, v. 73, no. 3, p. 287−310. doi:10.1007/BF00381447.

Johnson, E.A., 2006, Water in Nominally Anhydrous Crustal Minerals: Speciation, Concentration, and Geologic Significance. *in* Keppler, H. and Smyth, J.R., eds., Water in Nominally Anhydrous Minerals, Reviews in Mineralogy and Geochemistry 62 62, p.117−154. doi:10.2138/rmg.2006.62.6.

Krishnamurthy, P., 1974, Petrological and chemical studies of Deccan Trap lavas from western India. PhD Thesis, University of Edinburgh, 267 p.

Krishnamurthy, P., Gopalan, K., and MacDougall, J.D., 2000, Olivine Compositions in Picrite Basalts and the Deccan Volcanic Cycle. Journal of Petrology, v. 41, no. 7, p. 1057−1069. doi:10.1093/petrology/41.7.1057.

Larsen, L.M., and Pedersen, A.K., 2009, Petrology of the Paleocene Picrites and Flood Basalts on Disko and Nuussuaq, West Greenland. Journal of Petrology, v. 50, no. 9, p. 1667−1711. doi:10.1093/petrology/egp048.

Le Bas, M.J., Le Maitre, R.W., Streckeisen, A., and Zanettin, B.A., 1986, Chemical classification of volcanic rocks based on the total alkali-silica diagram. Journal of Petrology, v. 27, p. 745−750. doi:10.1093/petrology/27.3.745

Lejeune, A., and Richet, P., 1995, Rheology of crystal-bearing silicate melts: An experimental study at high viscosities. Journal of Geophysical Research: Solid Earth, v. 100, p. 4215−4229. doi:10.1029/94JB02985.

Lewis, J.D., and Williams, J.R., 1973, The petrology of an ultramafic lava near Murphy Well, Eastern Goldfields, Western Australia. Annual Report of the Geological Survey of Western Australia, v. 1972, p. 60−68.

Lightfoot, P.C., Hawkesworth, C.J., Hergt, J.M., Naldrett, A.J., Gorbachev, N.S., Fedorenko, V.A., and Doherty, W., 1993, Remobilisation of the continental lithosphere by a mantle plume: major-, trace-element, and Sr-, Nd-, and Pb-isotope evidence from picritic and tholeiitic lavas of the Noril'sk District, Siberian Trap, Russia. Contributions to Mineralogy and Petrology, v. 114, no. 2, p. 171−188. doi:10.1007/BF00307754.

Liu, J., Xia, Q., Kuritani, T., Hanski, E., and Yu, H., 2017, Mantle hydration and the role of water in the generation of large igneous provinces. Nature Communications, v. 8, no. 1, 1824. doi:10.1038/s41467-017-01940-3.

Miller, D.M., Langmuir, C.H., Goldstein, S.L., and Franks, A.L., 1992, The importance of parental magma composition to calc-alkaline and tholeiitic evolution: Evidence from Umnak Island in the Aleutians. Journal of Geophysical Research: Solid Earth, v. 97, p. 321−343. doi:10.1029/91JB02150.

Mueller, S., Llewellin, E.W., and Mader, H.M., 2010, The rheology of suspensions of solid particles. Proceedings of the Royal Society A: Mathematical, Physical and Engineering Sciences, v. 466, p. 1201−1228. doi:10.1098/rspa.2009.0445.

Natali, C., Beccaluva, L., Bianchini, G., Ellam, R.M., Savo, A., Siena, F., and Stuart, F.M., 2016, High-MgO lavas associated to CFB as indicators of plume-related thermochemical effects: The case of ultra-titaniferous picrite–basalt from the Northern Ethiopian–Yemeni Plateau. Gondwana Research, v. 34, p. 29−48. doi:10.1016/j.gr.2016.02.009.

Ni, H., Zheng, Y., Mao, Z., Wang, Q., Chen, R., and Zhang, L., 2017, Distribution, cycling and impact of water in the Earth's interior. National Science Review, v. 4, no. 6, p. 879−891. doi:10.1093/nsr/nwx130.

Nisbet, E.G., Cheadle, M.J., Arndt, N.T., and Bickle, M.J., 1993, Constraining the potential temperature of the Archaean mantle: A review of the evidence from komatiites. Lithos, v. 30, no. 3, p. 291−307. doi:10.1016/0024-4937(93)90042-B.

Norman, M.D., and Garcia, M.O., 1999, Primitive magmas and source characteristics of the Hawaiian Plume; petrology and geochemistry of shield picrites. Earth and Planetary Science Letters, v. 168, no. 1-2, p. 27−44.

Parman, S.W., Grove, T.L., Dann, J.C., and de Wit, M.J., 2004, A subduction origin for komatiites and cratonic lithospheric mantle. South African Journal of Geology, v. 107, no. 1−2, p. 107−118. doi:10.2113/107.1-2.107.

Plank, T., Kelley, K.A., Zimmer, M.M., Hauri, E.H., and Wallace, P.J., 2013, Why do mafic arc magmas contain ~4 wt% water on average? Earth and Planetary Science Letters, v. 364, p. 168−179. doi:10.1016/j.epsl.2012.11.044.

Portnyagin, M., Mironov, N.L., Matveev, S.V., and Plechov, P.Y., 2005, Petrology of avachites, high-magnesian basalts of Avachinsky Volcano, Kamchatka: II. Melt inclusions in olivine. Petrology, v. 13, no. 4, p. 322−351.

Renner, R., 1989, Cooling and crystallization of komatiite flows from Zimbabwe. Ph.D. Thesis, University of Cambridge, p.162.

Révillon, S., Arndt, N.T., Chauvel, C., and Hallot, E., 2000, Geochemical study of ultramafic volcanic and plutonic rocks from Gorgona Island, Colombia; the plumbing system of an oceanic plateau. Journal of Petrology, v. 41, no. 7, p. 1127−1153.

Rudnick, R.L., and Gao, S., 2003, Composition of the continental crust, in, Rudnick, R.L., ed., The Crust, Treatise on Geochemistry, Volume 3: Elsevier-Pergamon, Oxford, p. 1−64. doi:10.1016/b0-08-043751-6/03016-4.

Shaw, H.R., Wright, T.L., Peck, D.L., and Okamura, R., 1968, The viscosity of basaltic magma; an analysis of field measurements in Makaopuhi lava lake, Hawaii. Am J Sci, v. 266, no. 4, p. 225−264. doi:10.2475/ajs.266.4.225.

Sweeney, R.J., Falloon, T.J., Green, D.H., and Tatsumi, Y., 1991, The mantle origins of Karoo picrites. Earth and Planetary Science Letters, v. 107, no. 2, p. 256−271. doi:10.1016/0012-821x(91)90075-s.

Thompson, R.N., and Gibson, S.A., 2000, Transient high temperatures in mantle plume heads inferred from magnesian olivines in Phanerozoic picrites. Nature, v. 407, no. 6803, p. 502−506. doi:10.1038/35035058.

Truby, J.M., Mueller, S.P., Llewellin, E.W., and Mader, H.M., 2015, The rheology of three-phase suspensions at low bubble capillary number. Proceedings of the Royal Society A: Mathematical, Physical and Engineering Sciences, v. 471, 20140557. doi:10.1098/rspa.2014.0557.

Vigneresse, J.L., Barbey, P., and Cuney, M., 1996, Rheological Transitions During Partial Melting and Crystallization with Application to Felsic Magma Segregation and Transfer. Journal of Petrology, v. 37, no. 6, p. 1579−1600. doi:10.1093/petrology/37.6.1579.

Whattam, S.A., 2018, Primitive Magmas in the Early Central American Volcanic Arc System Generated by Plume-Induced Subduction Initiation. Frontiers in Earth Science, v. 6, 114. doi:10.3389/feart.2018.00114.

Wilson, A.H., 2003, A new class of silica enriched, highly depleted komatiites in the southern Kaapvaal Craton, South Africa. Precambrian Research, v. 127, no. 1, p. 125−141. doi:10.1016/S0301-9268(03)00184-0.

Yang, X., Deloule, E., Xia, Q., Fan, Q., and Feng, M., 2008, Water contrast between Precambrian and Phanerozoic continental lower crust in eastern China. Journal of Geophysical Research: Solid Earth, v. 113, no. B9. doi:10.1029/2007JB005541.